

Realization of highly efficient hexagonal boron nitride neutron detectors

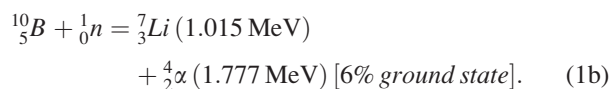
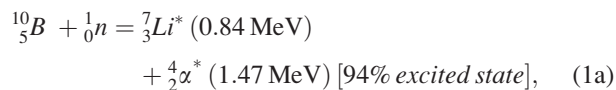
A. Maity, T. C. Doan, J. Li, J. Y. Lin, and H. X. Jiang^{a)}

Department of Electrical and Computer Engineering, Texas Tech University, Lubbock, Texas 79409, USA

(Received 9 July 2016; accepted 22 July 2016; published online 16 August 2016)

We report the achievement of highly efficient ^{10}B enriched hexagonal boron nitride ($h\text{-}^{10}\text{BN}$) direct conversion neutron detectors. These detectors were realized from freestanding 4-in. diameter $h\text{-}^{10}\text{BN}$ wafers 43 μm in thickness obtained from epitaxy growth and subsequent mechanical separation from sapphire substrates. Both sides of the film were subjected to ohmic contact deposition to form a simple vertical “photoconductor-type” detector. Transport measurements revealed excellent vertical transport properties including high electrical resistivity ($>10^{13}$ Ωcm) and mobility-lifetime ($\mu\tau$) products. A much larger $\mu\tau$ product for holes compared to that of electrons along the c -axis of $h\text{-BN}$ was observed, implying that holes (electrons) behave like majority (minority) carriers in undoped $h\text{-BN}$. Exposure to thermal neutrons from a californium-252 (^{252}Cf) source moderated by a high density polyethylene moderator reveals that 43 μm $h\text{-}^{10}\text{BN}$ detectors possess 51.4% detection efficiency at a bias voltage of 400 V, which is the highest reported efficiency for any semiconductor-based neutron detector. The results point to the possibility of obtaining highly efficient, compact solid-state neutron detectors with high gamma rejection and low manufacturing and maintenance costs. *Published by AIP Publishing.* [<http://dx.doi.org/10.1063/1.4960522>]

Hexagonal boron nitride ($h\text{-BN}$), an emerging wide band gap semiconductor with an energy bandgap of $E_g \sim 6.5$ eV, has been explored for its two dimensional nature and for its deep ultraviolet photonic device applications.^{1–8} It has a promising future in solid-state neutron detection as well.^{9–11} Due to the high thermal neutron capture cross-section (~ 3840 b) of ^{10}B atoms, ^{10}B enriched $h\text{-BN}$ ($h\text{-}^{10}\text{BN}$ or $h\text{-BN}$) has an absorption length of 47.3 μm for thermal neutrons. At large thicknesses, $h\text{-}^{10}\text{BN}$ can absorb 100% incident thermal neutrons. Detection of neutrons depends on the fission reaction between the neutrons and ^{10}B atoms.



Daughter particles (${}^7_3\text{Li}$, ${}^4_2\alpha$) created from nuclear reactions with large kinetic energies travel inside the material producing free electrons and holes which are collected as a signature for neutron detection. Therefore, $h\text{-BN}$ detectors are considered direct conversion detectors. Moreover, the large energy bandgap of $h\text{-BN}$ contributes to its extremely high electrical resistivity, which leads to a very low dark current density.^{5,10} Compared to B_4C ,¹² pyrolytic or polycrystalline BN, and alpha rhombohedral boron complexes,^{13,14} $h\text{-BN}$ has a simpler crystalline structure and hence epilayers produced by the epitaxy method possess higher crystalline quality and fewer defect-traps, providing excellent charge transport properties. The constituent atoms of BN have low atomic numbers, making it insensitive to gamma photons.¹⁰

^3He gas has long been the prime material for neutron detection. However, there are some shortcomings for gas-filled

detectors. Though ^3He has a higher thermal neutron capture cross-section (~ 5330 b), because it is a gas, it possesses very low atomic density which leads to long absorption length. Thus, ^3He gas detectors are bulky in nature. Other disadvantages include high voltage operation, low Q value (~ 0.764 MeV), and high ionization energy. Moreover, its scarcity has had an extreme effect on its price in recent days. Therefore, alternatives to ^3He gas detectors are highly desirable. Until now, the most effective solid-state detector approach has been the micro-structured semiconductor neutron detector (MSND), which has been reported extensively in recent years.^{15–17} This type of indirect conversion detector is composed of Si filled with either ^{10}B or ^6LiF . The detection efficiency depends upon microstructure design, material choice, and depth of the reacting material. The most efficient semiconductor based thermal neutron detector that has ever been reported consists of a ^{10}B filled Si microstructure with an efficiency of 48.5%.^{15,18} On the other hand, stacked ^6LiF filled Si detectors¹⁷ with a certified detection efficiency of 30% have already been commercialized.

Here, we report the attainment of ^{10}B enriched $h\text{-BN}$ neutron detectors with a record high detection efficiency of 51.4% for thermal neutrons. Detailed material synthesis and transport property characterization along with detector fabrication methods are described. Resistivity and photo-generated carrier mobility-lifetime products were measured to characterize the transport properties. Finally, the pulse height spectrum was recorded under thermal neutron irradiation from a Californium-252 (^{252}Cf) neutron source moderated by a high-density polyethylene (HDPE) moderator.

Thick films of ^{10}B enriched (99.9%) $h\text{-BN}$ were grown by metal organic chemical vapor deposition (MOCVD) on c -plane sapphire substrates. Trimethylboron (TMB) and ammonia (NH_3) were used as precursors for growth, and nitrogen was used as a carrier gas. Freestanding $h\text{-}^{10}\text{BN}$ films were obtained by mechanical separation of the substrates.

^{a)}Email: hx.jiang@ttu.edu

The fabricated neutron detectors reported here have a h - ^{10}B N layer thickness of $43\ \mu\text{m}$ and a size of $1\ \text{mm} \times 1\ \text{mm}$. E-beam evaporation was used to deposit ohmic bi-layer metal contacts of Ni (10 nm) and Au (20 nm) on both sides of the h - ^{10}B N film creating a simple vertical “photoconductor-type” device, as illustrated in Figs. 1(a) and 1(b).

^{10}B has a cross-section (σ) of 3840 b ($3.84 \times 10^{-21}\ \text{cm}^2$) for thermal neutrons (25 meV energy). The density of boron in h -BN is $5.5 \times 10^{22}\ \text{cm}^{-3}$. Thermal neutrons therefore have an absorption coefficient of $\alpha = N\sigma = 5.5 \times 10^{22} \times 3.84 \times 10^{-21} = 211.2\ \text{cm}^{-1}$ in 100% ^{10}B enriched h -BN films. Hence, the absorption length (λ) of thermal neutrons in h - ^{10}B N can be obtained as $\lambda = 1/\alpha = 1/211.2\ \text{cm} = 4.73 \times 10^{-3}\ \text{cm} = 47.3\ \mu\text{m}$. On the other hand, the thermal neutron absorption probability in an h - ^{10}B N film with a thickness, d , can be expressed as

$$P(d) = 1 - e^{-d/\lambda}. \quad (2)$$

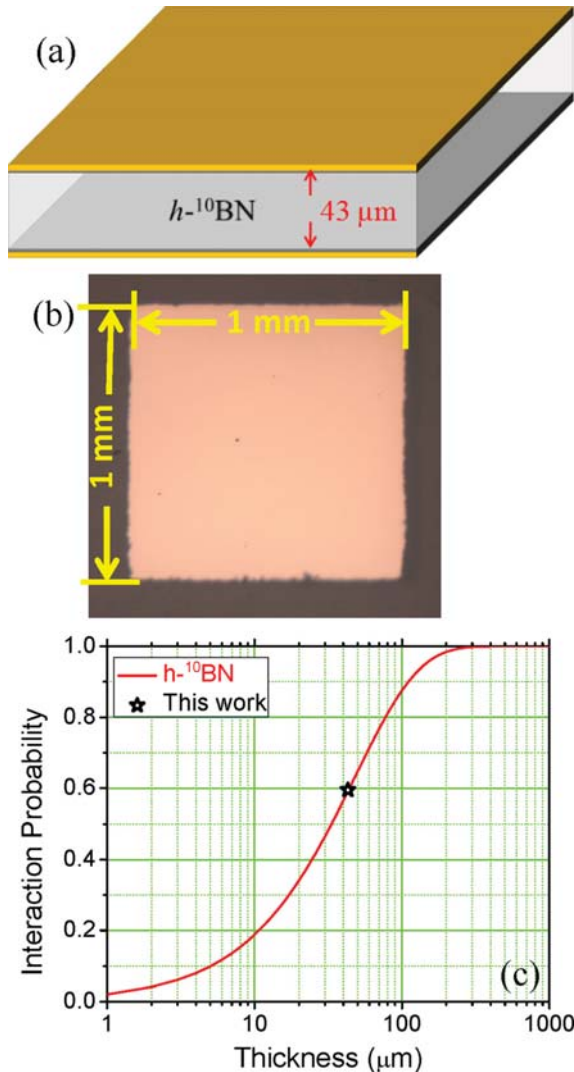


FIG. 1. (a) Schematic of cross-sectional view and (b) optical image of a fabricated $1\ \text{mm}^2$ size h - ^{10}B N thermal neutron detector consisting of a $43\ \mu\text{m}$ thick freestanding ^{10}B enriched h -BN epilayer. (c) Plot of thermal neutron interaction probability for 100% ^{10}B enriched h -BN with respect to film thickness according to Eq. (2).

A neutron detector consisting of a $43\ \mu\text{m}$ thick h - ^{10}B N epilayer can therefore absorb 59.7% of incident neutrons, as indicated in Fig. 1(c).

Materials were characterized in terms of the photo-generated carrier mobility-lifetime ($\mu\tau$) product and electrical resistivity (ρ). The $\mu\tau$ product can be visualized as the distance travelled by the carriers upon application of a unit electric field. In order to collect the excited free carriers at both the electrodes, the recombination lifetime (τ) of carriers must be longer than the transit time (τ_t), i.e., $\tau \geq \tau_t$, where $\tau_t = L/\mu E$. Here, E is the electric field applied and L is the spacing between the two ohmic contact electrodes (the thickness of the detector in this case), which is also the maximum travelling distance of carriers. This relation can be rewritten in terms of the mobility-lifetime product as $\mu\tau \geq L^2/V$ where V is the voltage applied between the two electrodes. Higher $\mu\tau$ products that translate to lower applied voltages needed to ensure maximum charge collection.

To measure the $\mu\tau$ products, a $1\ \text{mm} \times 1\ \text{mm}$ detector, as shown in Fig. 1(b), is illuminated with a broadband light source (LDLS, EQ-99 by Energetiq). Only the above band gap photons (wavelength $< 191\ \text{nm}$) are absorbed with a very short optical absorption length ($\sim 13\ \text{nm}$)^{5,19} compared to the sample thickness ($43\ \mu\text{m}$). Therefore, all of the electron-hole pairs are generated within the top few layers of h -BN, which allows us to measure $\mu\tau$ products for holes and electrons separately.²⁰ Two possible biasing conditions determine the transporting carrier type (holes or electrons). If the illuminated side of the device is connected to a positive contact (anode) of the bias voltage, then photo-generated electrons get swept out by the anode, and holes need to drift the entire thickness of the device to reach negative end (cathode) and vice versa. Thus, $\mu\tau$ products for holes and electrons can be separately measured from I–V characteristics under photoexcitation as described in Many’s equation.²⁰

$$I_i(V) = I_{0,i} \left[\frac{V\mu_i\tau_i \left(1 - e^{-\frac{L^2}{V\mu_i\tau_i}}\right)}{L^2 \left(1 + \frac{s_i L}{\mu_i V}\right)} \right]. \quad (i = e, h). \quad (3)$$

Here, V is the applied bias voltage between two electrodes, separated by a distance L , and $\mu_h\tau_h$ ($\mu_e\tau_e$) and s_h (s_e) are the mobility-lifetime product and surface recombination velocity for holes (electrons), respectively. This equation describes the trapping of carriers on the surface and inside of the material. By fitting the measured I–V curves under photoexcitation with Eq. (3), as shown in Fig. 2, the obtained $\mu_h\tau_h$ ($\mu_e\tau_e$) for holes (electrons) was 2.2×10^{-5} (8.3×10^{-7}) cm^2/V .

It is interesting to note that the measured $\mu_h\tau_h$ is much larger than $\mu_e\tau_e$. This is surprising by considering the fact that electrons and holes in single h -BN sheets have an equal effective mass^{7,21} and hence a comparable mobility. A much larger $\mu\tau$ product for holes compared to that of electrons indicates that the recombination lifetime of holes is much larger than that of electrons along the c -axis of h -BN, $\tau_h \gg \tau_e$. This observation is in fact consistent with our understanding that undoped h -BN, in which the quasi-Fermi level is below the middle of the energy bandgap, is more p-type in nature.^{22,23} Thus, holes (electrons) behave like majority (minority)

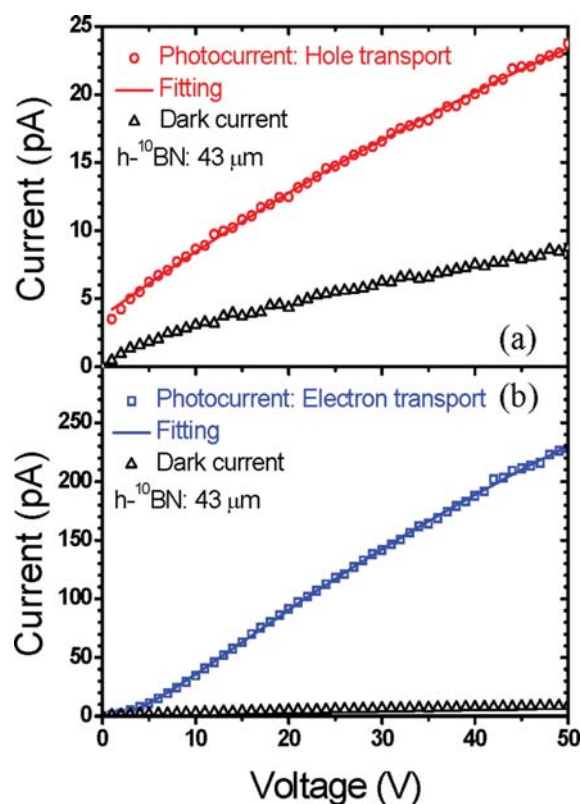


FIG. 2. I–V characteristics of a 1 mm^2 size neutron detector consisting of a $43 \mu\text{m}$ thick freestanding ^{10}B enriched $h\text{-BN}$ epilayer under light illumination: (a) Hole collection and (b) electron collection. The solid curves are least squares fitting of data with Eq. (3).

carriers in undoped $h\text{-BN}$. From the Einstein equation, the diffusion length L_D can be written as

$$L_D = \sqrt{\frac{K_B T}{q}} \mu \tau. \quad (4)$$

Here, K_B is the Boltzmann constant ($1.38 \times 10^{-23} \text{ m}^2 \text{ kg s}^{-2} \text{ K}^{-1}$), T is the measurement temperature, and q is charge of an electron ($1.6 \times 10^{-19} \text{ C}$). From Eq. (4), calculated diffusion lengths for holes and electrons are $7.6 \mu\text{m}$ and $1.5 \mu\text{m}$, respectively. Moreover, based on the dark I–V characteristics of hole transport and the device geometry (device area $A = 1 \text{ mm} \times 1 \text{ mm}$ and thickness $L = 43 \mu\text{m}$), the calculated electrical resistivity of $43 \mu\text{m}$ thick $h\text{-}^{10}\text{B}$ films exceeds $10^{13} \Omega \text{ cm}$.

A Californium-252 (^{252}Cf) neutron source with a radioactivity of 0.93 mCi ($4.0 \times 10^6 \text{ n/s}$) moderated by a 1 in. thick HDPE moderator was used to provide thermal neutrons as described in earlier works.^{10,11,24,25} Detection electronics were commercially obtained from Cremat Inc. and included a charge sensitive preamplifier and a Gaussian-shaping amplifier. A Gaussian shaped pulse is fed into a multichannel analyzer (MCA) (Amptek 8000D) to obtain the pulse height spectrum of the reaction conceived inside the $h\text{-BN}$ detector. Analog amplifiers are shielded from electronic noise inside an aluminum box along with the detector. A preamplifier (mode CR-110) is chosen for maximum amplification of the signal with minimum noise induction. A Gaussian shaping amplifier (model CR-200) with a $2 \mu\text{s}$ shaping time (FWHM

$4.7 \mu\text{s}$) is used for further amplification and pulse shape optimization. The experiment was set up in such a way that the detector to source distance was 30 cm as depicted in Fig. 3. The pulse height spectrum of the neutron response of our 1 mm^2 size ^{10}B enriched $h\text{-BN}$ detector was recorded at a bias voltage of 400 V for 10 min and is shown in Fig. 4. The corresponding “dark” response was also measured without any radiation exposure under the same conditions. Gamma exposure from Caesium-137 (^{137}Cs) proved unresponsiveness of $h\text{-BN}$ detectors to gamma photons.

Neutrons are counted one at a time due to the very low rate of incident neutrons on the detector compared to the response time of the detection system with a FWHM of the output Gaussian pulse of $4.7 \mu\text{s}$. Daughter particles produced from a nuclear reaction travel inside the $h\text{-BN}$ film generating electron-hole clouds on their way. Li and α particles both have short ranges (about $2 \mu\text{m}$ for Li and about $5 \mu\text{m}$ for α ^{26,27}) in $h\text{-BN}$ compared to the device thickness and therefore deposit all their energies inside $h\text{-BN}$. When applied electric field in the detector is sufficiently strong, all charge carriers are collected on the electrodes within a very short time, which is integrated in the charge sensitive preamplifier generating a voltage pulse at the output. This voltage pulse is then amplified and shaped in Gaussian shaping amplifier. Each pulse therefore corresponds to one neutron absorbed and placed at a certain channel by the MCA.

The total neutron count was obtained by integrating the spectrum beyond the highest channel of dark response, which effectively acted as a low-level discriminator (LLD). The thermal neutron response of the $h\text{-}^{10}\text{B}$ detector was calibrated against a commercially purchased ^6LiF filled micro-structured semiconductor neutron detector (MSND) from Radiation Detection Technologies, Inc. This MSND (DominoTM V4) of model D411S-30-D0010-V4 was specified with a detection efficiency of 30% for thermal neutrons with a device area of 4 cm^2 . A count rate of 0.77 n/s was obtained for our 1 mm^2 size $h\text{-}^{10}\text{B}$ detector, which gives a count rate per unit area of 77.2 n/s cm^2 under the above stated conditions. As depicted in Fig. 3, the ^6LiF filled MSND was placed at the same location as the $h\text{-BN}$ detector (30 cm from ^{252}Cf source) for 10 min furnishing a count rate of 180.4 n/s , corresponding to a count rate

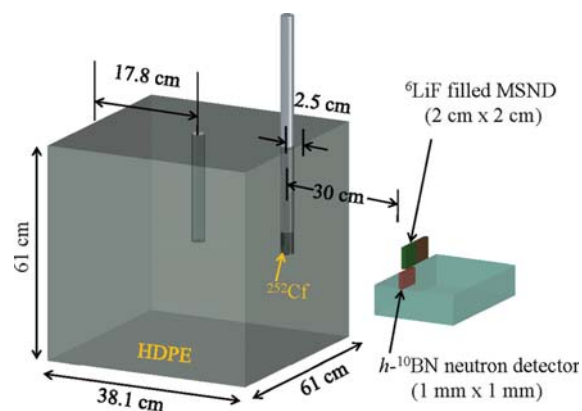


FIG. 3. Schematic diagram of the experimental setup for pulse height spectra and detection efficiency measurements. The ^{252}Cf source is placed in the outer hole of HDPE, 2.5 cm away from the surface. The distance from the ^{252}Cf source to the $h\text{-}^{10}\text{B}$ detector and ^6LiF filled MSND is fixed at 30 cm .

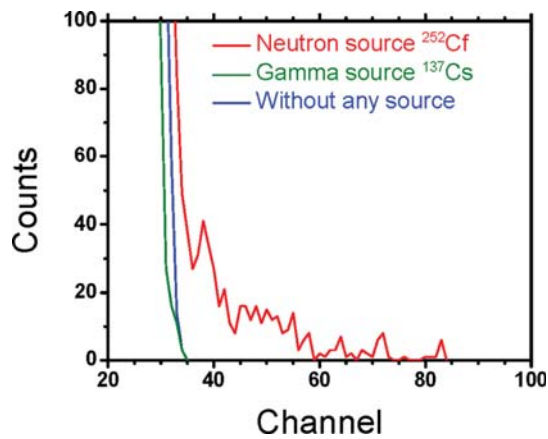


FIG. 4. Pulse height spectrum under neutron irradiation measured with a 1 mm^2 size neutron detector consisting of a $43\text{ }\mu\text{m}$ thick freestanding ^{10}B enriched $h\text{-BN}$ epilayer biased at a voltage of 400 V measured for 10 min . Blue color indicates background counts without any radiation source. Red color indicates neutron counts in response to ^{252}Cf moderated by an HDPE moderator and green color depicts response from a gamma source of ^{137}Cs .

per unit area of 45.1 n/s cm^2 . Comparing the count rates of the $h\text{-BN}$ detector and the ^6LiF filled MSND detector, thermal neutron detection efficiency of our $43\text{ }\mu\text{m}$ thick 1 mm^2 size ^{10}B enriched $h\text{-BN}$ detector can be obtained via the following proportionality relation:

$$\eta_{^{10}\text{BN}} = \frac{C_{^{10}\text{BN}}}{C_{\text{MSND}}} \times \eta_{\text{MSND}}, \quad (5)$$

where $\eta_{^{10}\text{BN}}$ and $C_{^{10}\text{BN}}$ denote, respectively, the detection efficiency and the count rate per unit area of the $h\text{-}^{10}\text{BN}$ detector ($=77.2\text{ n/s cm}^2$); whereas η_{MSND} and C_{MSND} , respectively, denote the detection efficiency and the count rate per unit area of the ^6LiF filled MSND ($=45.1\text{ n/s cm}^2$). We therefore obtain the detection efficiency of the ^{10}B enriched $h\text{-BN}$ detector as

$$\eta_{^{10}\text{BN}} = \frac{77.2}{45.1} \times 30\% = 51.4\%.$$

As a film $43\text{ }\mu\text{m}$ thick $h\text{-}^{10}\text{BN}$ can absorb 59.7% of incident thermal neutrons, the results imply that the charge collection efficiency of our $h\text{-}^{10}\text{BN}$ detector is 86.1% at a bias voltage of 400 V . Additional improvements to the $\mu\tau$ products of electrons and holes in $h\text{-BN}$ epilayers are needed in order to further advance the charge collection efficiency. Moreover, theoretical studies that are capable of providing the intrinsic diffusion lengths and mobility-lifetime products for holes and electrons in $h\text{-BN}$ are highly desirable, as the results would provide valuable insights into how much future improvement one might expect as growth conditions and crystal quality are optimized.

In summary, we have demonstrated a highly efficient thermal neutron detector with 51.4% detection efficiency, which is record high among all semiconductor thermal neutron detectors. Thick ^{10}B enriched $h\text{-BN}$ grown by the epitaxy method exhibits excellent carrier transport properties, achieving 86.1% charge collection efficiency at a relatively moderate bias voltage of 400 V . A much larger $\mu\tau$ product for holes compared to that of electrons along the c -axis of

$h\text{-BN}$ was observed, which infers that holes (electrons) behave like majority (minority) carriers in undoped $h\text{-BN}$. The high resistivity and excellent transport properties of charge carriers of $h\text{-BN}$ will allow us to scale the detectors to larger sizes. The demonstrated outstanding electrical properties and performance of thick ^{10}B enriched $h\text{-BN}$ detectors ensure that highly efficient, compact solid-state neutron detectors with low manufacturing and maintenance costs are feasible and they could eventually replace ^3He gas-filled detectors.

The support from the DHS ARI Program (2011-DN-077-ARI048) and the DOE NNSA SSAA program (DE-NA0002927) made research efforts on $h\text{-BN}$ material growth and neutron detector fabrication possible. The study of the basic structural properties of $h\text{-BN}$ is supported by the NSF (ECCS-1402886). Jiang and Lin are grateful to the AT&T Foundation for the support of Ed Whitacre and Linda Whitacre Endowed chairs.

- ¹K. Watanabe, T. Taniguchi, and H. Kanda, *Nat. Mater.* **3**, 404 (2004).
- ²Y. Kubota, K. Watanabe, O. Tsuda, and T. Taniguchi, *Science* **317**, 932 (2007).
- ³K. Watanabe, T. Taniguchi, T. Niiyama, K. Miya, and M. Taniguchi, *Nat. Photonics* **3**, 591 (2009).
- ⁴K. Watanabe and T. Taniguchi, *Phys. Rev. B* **79**, 193104 (2009).
- ⁵J. Li, S. Majety, R. Dahal, W. P. Zhao, J. Y. Lin, and H. X. Jiang, *Appl. Phys. Lett.* **101**, 171112 (2012).
- ⁶S. Majety, J. Li, X. K. Cao, R. Dahal, B. N. Pantha, J. Y. Lin, and H. X. Jiang, *Appl. Phys. Lett.* **100**, 061121 (2012).
- ⁷X. K. Cao, B. Clubine, J. H. Edgar, J. Y. Lin, and H. X. Jiang, *Appl. Phys. Lett.* **103**, 191106 (2013).
- ⁸R. Dahal, J. Li, S. Majety, B. N. Pantha, X. K. Cao, J. Y. Lin, and H. X. Jiang, *Appl. Phys. Lett.* **98**, 211110 (2011).
- ⁹J. Li, R. Dahal, S. Majety, J. Y. Lin, and H. X. Jiang, *Nucl. Instrum. Methods Phys. Res., Sect. A* **654**, 417 (2011).
- ¹⁰T. C. Doan, S. Majety, S. Grenadier, J. Li, J. Y. Lin, and H. X. Jiang, *Nucl. Instrum. Methods Phys. Res., Sect. A* **748**, 84 (2014).
- ¹¹T. C. Doan, S. Majety, S. Grenadier, J. Li, J. Y. Lin, and H. X. Jiang, *Nucl. Instrum. Methods Phys. Res., Sect. A* **783**, 121 (2015).
- ¹²K. Osberg, N. Schemm, S. Balkir, J. O. Brand, M. S. Hallbeck, P. A. Dowben, and M. W. Hoffman, *IEEE Sens. J.* **6**, 1531 (2006).
- ¹³D. S. McGregor, T. C. Unruh, and W. J. McNeil, *Nucl. Instrum. Methods Phys. Res., Sect. A* **591**, 530 (2008).
- ¹⁴A. N. Caruso, *J. Phys.: Condens. Matter* **22**, 443201 (2010).
- ¹⁵Q. Shao, L. F. Voss, A. M. Conway, R. J. Nikolic, M. A. Dar, and C. L. Cheung, *Appl. Phys. Lett.* **102**, 063505 (2013).
- ¹⁶K.-C. Huang, R. Dahal, J. J.-Q. Lu, A. Weltz, Y. Danon, and I. B. Bhat, *Nucl. Instrum. Methods Phys. Res., Sect. A* **763**, 260 (2014).
- ¹⁷S. L. Bellinger, R. G. Fronk, W. J. McNeil, T. J. Sobering, and D. S. McGregor, *IEEE Trans. Nucl. Sci.* **59**, 167 (2012).
- ¹⁸A. M. Conway, R. J. Nikolic, and T. F. Wang, in *Proceedings of the International Semiconductor Device Research Conference* (IEEE, New York, 2007), p. 589.
- ¹⁹T. Sugino, K. Tanioka, S. Kawasaki, and J. Shirafuji, *Jpn. J. Appl. Phys., Part 2* **36**, L463 (1997).
- ²⁰A. Many, *J. Phys. Chem. Solids* **26**, 575 (1965).
- ²¹G. W. Semenov, *Phys. Rev. Lett.* **53**, 2449 (1984).
- ²²T. C. Doan, J. Li, J. Y. Lin, and H. X. Jiang, *AIP Adv.* **4**, 107126 (2014).
- ²³X. Z. Du, J. Li, J. Y. Lin, and H. X. Jiang, *Appl. Phys. Lett.* **108**, 052106 (2016).
- ²⁴J. Clinton, "Optimization and characterization of a novel shelf powered solid state neutron detector," Ph.D. thesis, Rensselaer Polytechnic Institute, New York, USA, 2011, Chap. 3, pp. 73–78.
- ²⁵R. Dahal, K. C. Huang, J. Cliton, N. LiCausi, J.-Q. Lu, Y. Danon, and I. Bhat, *Appl. Phys. Lett.* **100**, 243507 (2012).
- ²⁶G. F. Knoll, *Radiation Detection and Measurement*, 4th ed. (John Wiley & Sons, 2010).
- ²⁷F. P. Doty, "Boron nitride solid state neutron detectors," U.S. patent 6,727,504 (2004).